LA-UR-14-24722
Approved for public release; distribution is unlimited.

Title: Ejecta Particle-Size Measurements in Vacuum and Helium Gas using Ultraviolet In-Line Fraunhofer Holography

Author(s): Sorenson, Danny S.; Pazuchanics, Peter; Johnson, Randall P.; Malone, R.M.; Kaufman, M.I.; Tibbitts, A.; Tunnell, T.; Marks, D.; Capelle, G.A.; Grover, M.; Marshall, B.; Stevens, G.D.; Turley, W.D.; LaLone, B.

Intended for: Report

Issued: 2014-06-25

(U) Ejecta Particle-Size Measurements in Vacuum and Helium Gas using Ultraviolet In-Line Fraunhofer Holography

D. S. Sorenson, P. Pazuchanics, R. Johnson
Los Alamos National Laboratory, Los Alamos, NM

R. M. Malone, M. I. Kaufman, A. Tibbitts, T. Tunnell, D. Marks
NSTec, LLC, Los Alamos, NM

G. A. Capelle, M. Grover, B. Marshall, G. D. Stevens, W. D. Turley, B. LaLone
NSTec, LLC, Special Technologies Laboratory, Santa Barbara, CA

An Ultraviolet (UV) in-line Fraunhofer holography diagnostic has been developed for making high-resolution spatial measurements of ejecta particles traveling at many mm/μsec. This report will discuss the development of the diagnostic including the high-powered laser system and high-resolution optical relay system. In addition, the system required to reconstruct the images from the hologram and the corresponding analysis of those images to extract particles will also be described. Finally, results from six high-explosive (HE), shock-driven Sn ejecta experiments will be presented. Particle size distributions will be shown that cover most of the ejecta velocities for experiments conducted in a vacuum, and helium gas enviroments. In addition, a modification has been made to the laser system that produces two laser pulses separated by 6.8 ns. This double-pulsed capability allows a superposition of two holograms to be acquired at two different times, thus allowing ejecta velocities to be measured directly. Results from this double pulsed experiment will be described.

1. INTRODUCTION:

When a shock wave interacts at a metal vacuum interface "ejected matter" (ejecta) can be emitted from the surface. The mass, size, shape, and velocity of the ejected material depends on the initial shock conditions, material properties of the shocked metal surface, and the surface roughness. A variety of measurement techniques have been developed to determine the properties of ejecta. Radiography, [1-2] PZT and $LiNbO_3$ pins,[3-5] and Asay foils[6-8] have been used to determine areal mass densities. Visible imaging and shadowgraphy have been used to measure the spatial extent of ejecta clouds (this measurement being extremely sensitive to the smallest amounts of ejecta particles). For determining ejecta particle-size distributions, an in-line Fraunhofer holography[9] has been used. This measurement technique was first developed at Lawrence Livermore National Laboratory (LLNL) in the late 1980s,[10] and at Los Alamos National Laboratory (LANL) in the 1990s.[11-12] The LANL effort was carried out in support of the High Energy Density Physics and subcritical experiments. These holography measurements were costly and time consuming, though returned excellent data. To achieve resolution of a few microns, costly lens systems were sacrificed for each experiment,[a] thus driving the cost and setup time up for these experiments. In addition, many of the experiments did not have the resolution to determine the peak of the particle size distribution, as the distribution was still rising at the resolution limit. Since those earlier experiments, many technological advances have been made that presented the opportunity for significant improvements in the measurement technique. In particular, the advances in laser systems and computing capabilities have made an extremely difficult measurement and analysis much simpler and cost effective. Because of these technological advances, in 2008 a new holography project was initiated to improve the resolution

[a] To achieve high resolution, a low F# lens system is required which physically puts the front lens element very close to the physics package which will typically be destroyed when the experiment is executed.

of the current measurement technique. One of the goals for the project was to extend the resolution of the system from near 2.0 microns in diameter to 0.5 microns in diameter. Another goal for the project was to design the experiments to allow the full velocity distribution to be measured. Finally, in addition to improving the overall quality of the data, the experiments would be designed in such a way as to be cost effective, allowing for many experiments to be conducted in a short period of time.[b] In this report, a new high-resolution UV in-line Fraunhofer holography experiment technique will be described. In addition, ejecta particle size distributions will be presented from a variety of recent experiments that were conducted in both vacuum and helium gas environments. Finally, a double-pulsed holography experiment will be presented. This was accomplished by modifying the high-powered laser in which the laser beam pulse was split into two laser beam pulses with half the energy. One of these pulses is then delayed relative to the other and are recombined thus providing two pulses on the same optical axis separated in time. This process allows a double-pulsed hologram to be recorded, allowing ejecta particle velocities to be measured directly.

2. EXPERIMENTAL ARRANGEMENT

2.1 In-line Fraunhofer Holography

A measurement of the size, shape and position of small particles is a difficult proposition. The problem becomes significantly more difficult when the particles are traveling at many mm/µsec. Standard imaging techniques only work well when a single well-defined plane is being imaged. For example, a microscope system has a depth of field given by D^2/λ, where D is the diameter of the particler, and λ is the wavelength of light. For a 1-micron particle and $\lambda = 532$ nm, the depth of field is only 1.9 µm. One experimental technique that offers the ability to record a three-dimensional (3D) volume of particles is holography. Holographic techniques have been used for a variety of applications for many years, and are fundametnlally a 3D recording technique. Many variations of holography have been used to measure particle fields and the in-line Frauhofer holography is the technique adopted for measuring ejecta particles. Figure 2.1.1 shows a schematic of the technique. In the figure, a laser beam propagates from left to right through the volume of ejecta particles. Some of the light scatters from the particles and some is unscattered. These two wavefronts interfere at the film plane to form the hologram. One of the advantages of the in-line Frauhofer technique is that only one laser beam is required. For dynamic experiments in which particles can be traveling many mm/µsec, this

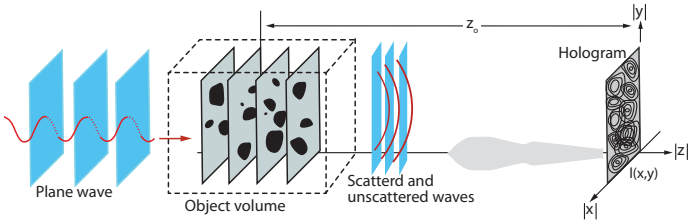

Fig. 2.1.1. Illustration of the in-line Fraunhofer holography technique. A laser beam impinges the particles in the object volume and some of the light is scattered and some of the light is unscattered. The two wavefronts interfere at the film to form the hologram a distance z_0 from the object volume.

technique removes a considerable complication of the standard holography technique in which two seperate beams are required. For example, in setting up a standard two-beam holography measurement, the object beam is used to scatter off the object being investigated and the reference beam is used to interfere with the scatterred beam to form the hologram. However, for dyamic experiments, in which the laser pulse width is 150 psec, this process requires the two path lengths to be equal within a ~ 100 microns, so the object and reference beams can combine and interfere. This stringent requirement for the object and reference beam path lengths create an additional complication in the setup of the experiment.

For the shock physics experiments discussed in this report, a high explosive is used to generate the shock wave in the metal. The energy released from the HE poises another significant complication for performing holography measurements of dynamic events. In order to achieve high resolution (near 1 micron), the in-line Fraunhofer technique would require the holographic film to be located about 1 mm from the volume of particles. This positioning of the film is not possible and the film would inevitably be destroyed. To deal with this issue, optical relay systems can be used to relay the object volume some distance to where the film will survive the experiment. However, the lens system or part of the lens system will likely be destroyed. This configuration is shown in Fig. 2.1.2. The top of the figure is similar to the previous figure, but now a lens system is inserted between the object volume and the holographic film. The schematic of the lens at the bottom of the figure is the actual lens assembly that is used for the experiments described in this report, and the lens system relays the object volume a distance of about 127 cm.

2.2 Experimental Setup at the Special Technologies Laboratory

In developing this new diagnostic, the Special Technologies Laboratory (STL) was used to carry out the development

[b] Typically one to two experiments per day.

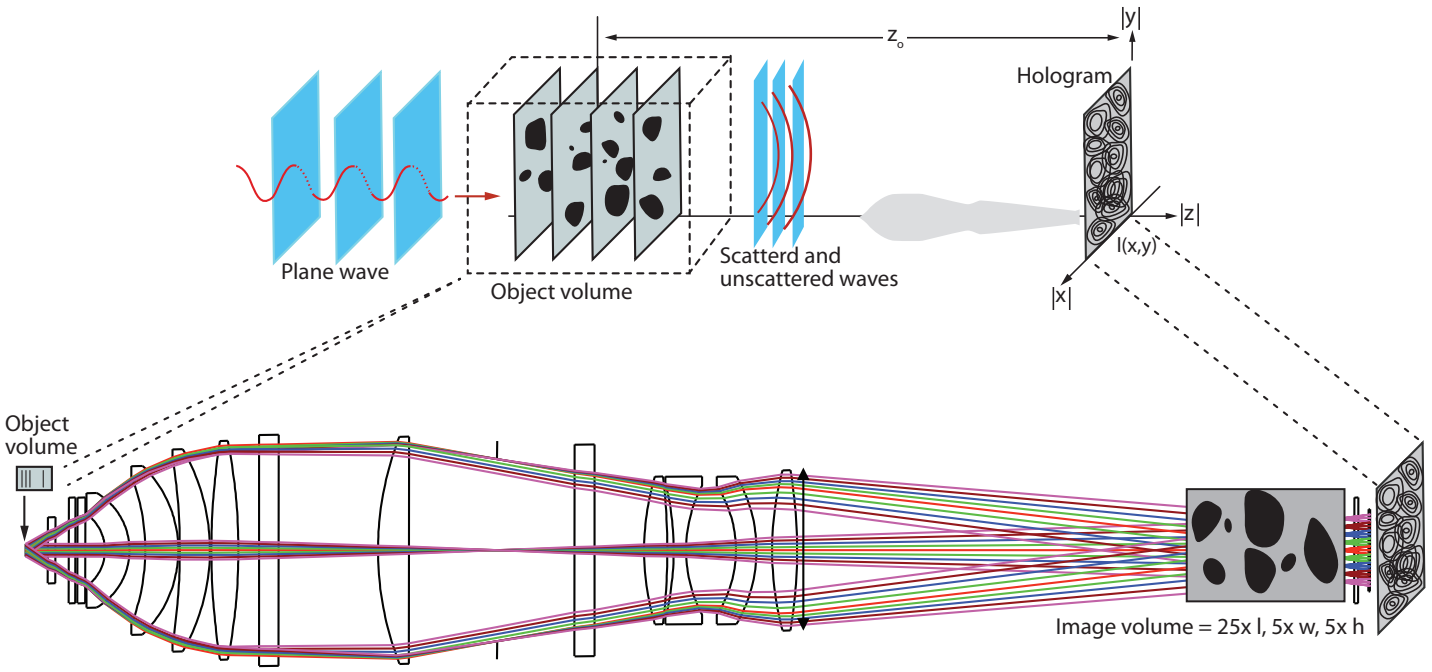

Fig. 2.1.2. The in-line Fraunhofer technique is adapted to be used to measure particles in a dynamic shock physics expeirment. A high-resolution lens system is located just after the object volumen as illustrated in the figure. The lens system relays the scattered and unscattered wavefronts some distance from the high-explosive experiment to where the hologram can be formed without being damaged. The lower part of the figure shows the lens system and the object volumen being relayed with magnification of 5 to a location just in front of the film.

of the diagnostic and conduct the dynamic experiments. In addition, NSTec personnel both from STL and Los Alamos Operations (LAO) supplied much of the support for the experiments. The facility makes use of a cylindrical vessel with an inner diameter of 43.2 cm and usable inner length of 61.0 cm. Figure 2.2.1 shows two drawings of the vessel. In the figure, there are two diagnostic ports with an opening of 12.3 cm. The vessel has been rated for 10 grams of high explosive, and is located in a separate room, as shown in the top right of Fig 2.2.2. The vessel can be moved as needed and, for the holography experiment, the vessel is orientated as shown. Also shown in the figure is the location of the high-powered laser which is located in an adjacent room. In this configuration, the 20-mm-diameter laser beam passes from the laser room into the vessel room. The laser beam enters the vessel through a series of mirrors and a 5.08-cm-diameter laser window mounted on the left side of the vessel. The beam continues through another 5.08-cm-diameter window that is mounted on the physics package. The beam then impinges on the ejecta particles. The scattered and unscattered waves pass through the exit window on the physics package and are relayed through the lens system as shown in the top of Fig. 2.2.3. The object volume is relayed 127 cm with a magnification of 4.97, as indicated in the bottom of the figure. The film is located just in front of the relayed image volume, as shown in the figure, where the scattered and unscattered wave fronts interfere at the film plane to form a hologram.

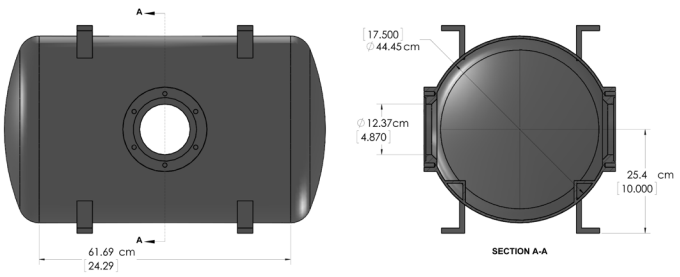

Fig. 2.2.1. Drawing of the vessel used for the HE experiments. The laser beam enters the vessel through one of the access ports, and the lens system is mounted on the opposited side.

2.2.1 Physics Package Design

As seen in Fig. 2.2.4 , the first lens element is in very close proximity to the experimental physics package, making it susceptible to being damaged after each experiment. The focal length distance is 78 mm, which is measured from the inside surface of the first lens element to the object plane (or 42.40 mm as measured from the outside surface of the front window). Figure 2.2.4 shows a detailed drawing of the physics package integrated with the vessel and the lens system. As seen in the figure, the physics package is only a few millimeters from the front flange of the lens system.

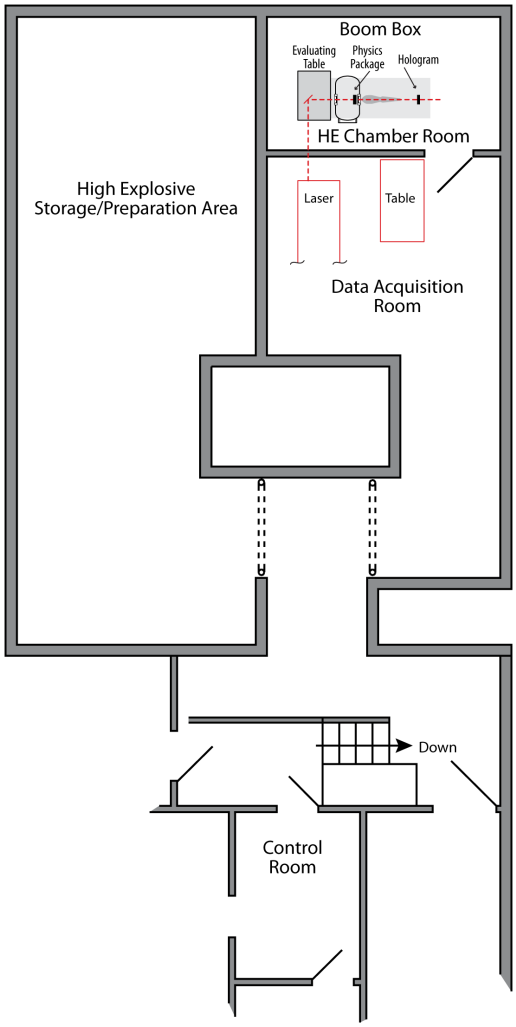

Fig. 2.2.2. "Boom Box" facility layout. The control room where the experiment is executed is shown at the bottom of the figure. The laser system is located in a seperate room indicated, and some of the experimental setup is shown in the room where the vessel is located (in the top right room of the figure).

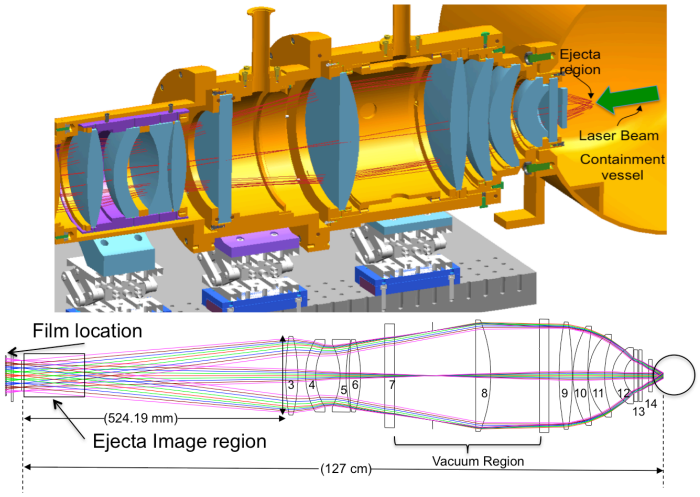

Fig. 2.2.3. Top of the figure is a model drawing of the lens system mounted to the vessel. A detailed cross section of the lens system is shown at the bottom of the figure.

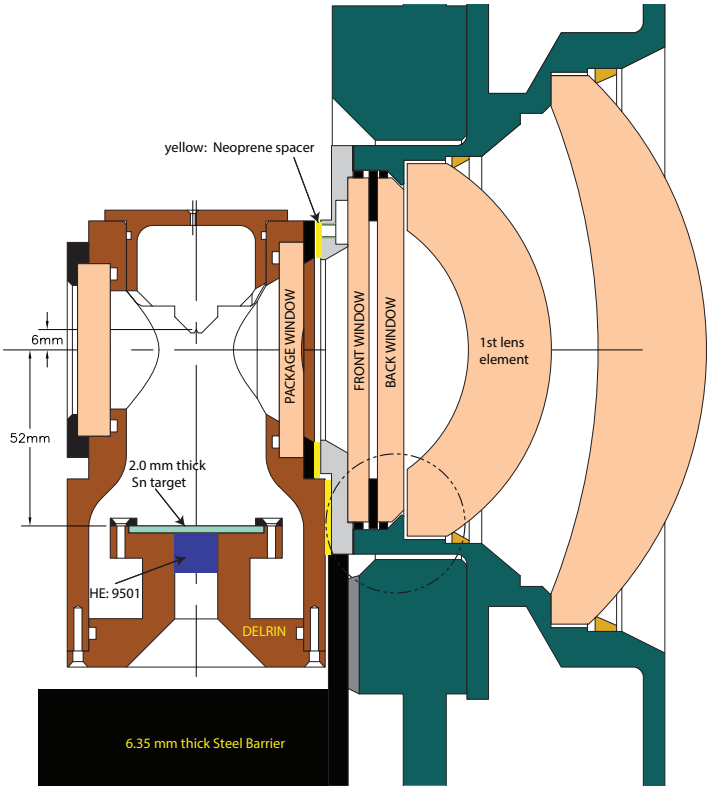

Fig. 2.2.4. Cross section drawing showing the experimental physics package in shot configuration and how it is integrated with the vessel and lens system.

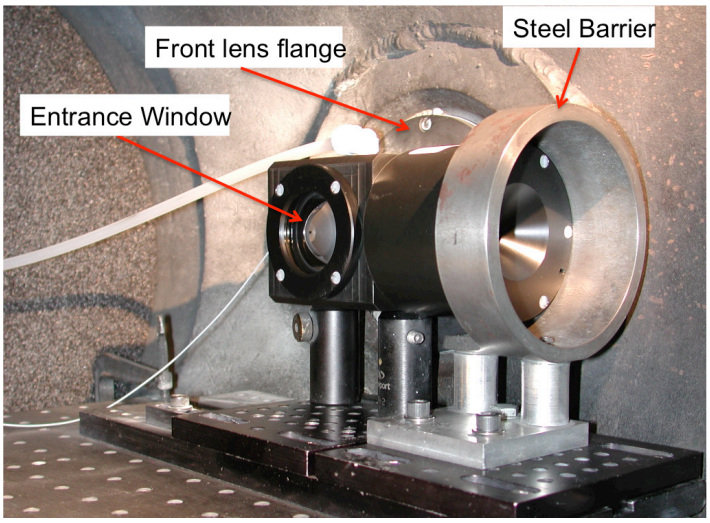

Fig. 2.2.5. Photograph of the experimental physics package inside the vessel just before an experiment.

Figure 2.2.5 shows a photograph of the physics package just before an experiment. The laser beam travels from left to right entering the physics package entrance window as indicated in the figure. Because of the close proximity of the HE to the lens system, a variety of shock and fragment mitigation features were designed into the package and how it coupled to the vessel and lens system. Referring back to Fig. 2.2.4, the inside of the package was enlarged so that

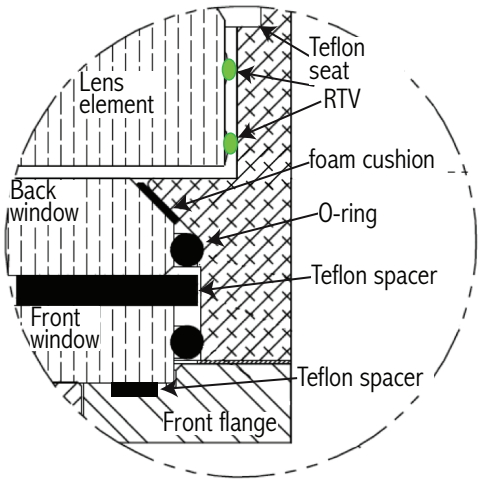

Fig. 2.2.6. Details of new front end lens housing assembly. The circular region is identified in figure 2.2.4.

the 40-mm-diameter target can freely move in the forward direction. This configuration prevents the fast moving target from hitting the sides of the package, producing secondary fragments that might hit the front window of the lens system. Figure 2.2.6 shows a detailed drawing of how the two windows in front of the first lens element are mounted into the lens housing. The two windows are separated by a gap using a Teflon washer as indicated. The gap between the windows decouples one window from the other, preventing the front window (that gets hit and fragments) from transmitting the energy directly into the secondary window (which is designed to protect the first lens element L12). In addition, O-rings are used on the outer diameter of the windows as indicated in the figure to decouple the lens housing from the windows, mitigating the energy transfer from the windows to the lens housing. Finally, the windows are held into position by three Teflon spacers (one is shown in the figure). The Teflon spacers have set screws (not shown) that push the window assembly against a foam cushion. By adjusting these three set screws the tilt of the windows can be adjusted. The figure also shows that the first lens element is set back from the back window with a air gap and is mounted into the lens housing with Room Temperature Volcanizing (RTV) silicon, and seated against a Teflon spacer. In addition to this mounting strategy of the lens element, both the glass and fabrication of the lens element were changed from a previous design. Details of these changes are discussed later on in the report. All indications are that the design changes have proven successful in that the lens has not been damaged after 25 experiments.

Referring back to Fig. 2.2.4, special attention was given to how the physics package was configured in the vessel for the experiment. In particular, neoprene washers were used to fill the gap between the experimental physics package and the flange. In addition, the package was rigidly mounted to a plate that is firmly mounted in the vessel. Finally, a

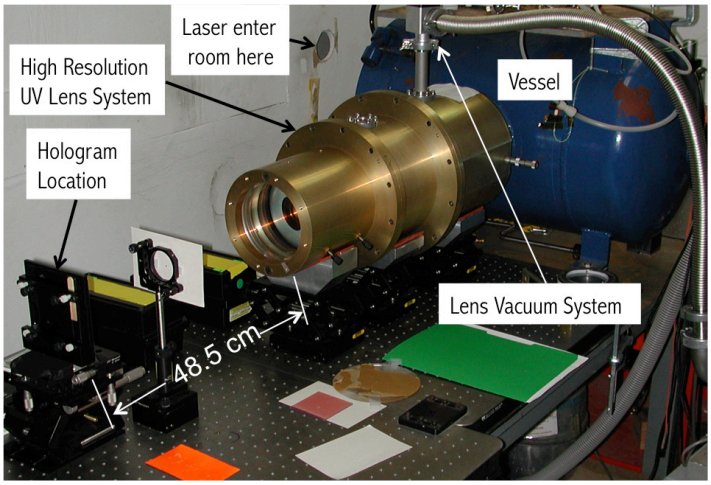

Fig. 2.2.7. Photograph of holography experiment just before and experiment.

Steel barrier was designed to fill the gap between the lower section of the physics package and the vessel wall. This barrier prevented the bulk of the physics package from making contact with the vessel flange, mitigating both fragments and shocks that might couple into the holography lens system. The front protection window is replaced routinely after every experiment and has been observed to suffer very minor pitting all the way to being completely shattered. The second window rarely has to be replaced, but can easily be done if needed.

A photograph of a typical experimental setup is shown in Fig. 2.2.7. The lens system is shown after it has been mounted to the flange of the vessel. Once the lens system is aligned and mounted to the vessel, it is not removed until after the experimental campaign has completed. Not shown in the figure are two lasers used to aid the alignment of the lens system. The hologram location is shown at the far left of the figure. A narrow band filter, used to block any unwanted light from the experiment, is shown in the figure located just in front of the holographic film. The distance the hologram is located from the lens system is shown at 48.5 cm which is close to the focal length (49.0 cm) of the lens. As the ejecta plane is located roughly 1.5 mm in front of the front focal length of the lens, this object plane will be relayed (with a magnification of 25 along the optical axis) to 32.5 mm in front of the hologram. In order to monitor the timing and performance of the high-power laser, two light monitors (not shown in the figure) are used to measure the laser pulse produced at the laser and at the holographic film. Finally, a velocimetry measurement using Photon Doppler Velocimetry (PDV)[13] is made on every experiment. The recording setup for the experiment is shown in Appendix 1 along with the free surface velocity measurement as measured from the PDV diagnostic.

2.3 High-Resolution Optical Relay System

In order to improve the resolution of the holography measurement, the laser light used for the measurement was decreased from 532 nm to 355 nm.[c] This change can potentially improve the resolution of the measurement by the ratio of the wavelengths. In addition to the wavelength change, a new optical relay system was designed to work at this wavelength. Furthermore, because the lens was expected to survive each experiment, more effort was spent in optimizing the resolution of the system. The lens system,[14-15] which is calculated to give 2000 lp/mm at 20% modulation with an f/# of 0.89 will be described below.

Because a high powered collimated laser beam travels through the lens system, the lens design needed to accomadate for the focus of the laser beam inside the lens assembly. The focus of the laser beam in air produces enough energy density to ionize the the air, destroying the the uniform phase of the reference beam. Therefore the lens system was designed so that a vacuum region existed in the lens system. In Fig 2.3.1 this region is located between the two vacuum windows. Careful collimation of the laser is required so as not to have the focus move from the designed location to a positon close to an optical surface, where the anti-reflection coating would be damaged. Another design feature for the lens system is the magnification. The current design of the lens has a magnification of 5. This has the benefit of reducing the film requirements by that factor. The holographic film used for these experiments, the film has a recording capability of 3000 lp/mm resolution. So, if the ejecta region is magnified by 5X by the lens, the resolution of the relayed image to be recorded is 400 lp/mm. If the diameter of the areal region of ejecta particles is 12 mm, then at the holographic film its image will be increased to 60 mm. Standard sized holographic film measures 76 x 76 mm. For this design, the reference laser beam is larger than the 60 mm diameter image, allowing adequate recording of interference fringes. Figure 2.3.1 shows that the ejecta volume measures 12-mm diameter and 5-mm deep. This volume is relayed to the image region that measures 60-mm diameter and 125-mm deep. Although the x and y magnification is 5X, the z magnification is 25X. So, a 1-μm spherical ejecta particle is relayed as a cylindrical particle measuring 5-μm cylindrical diameter by 25-μm long. During the reconstruction of the hologram, it is the centroid and position of this cylindrical particle that is measured.

Figure 2.3.2 shows that the resolution for recording ejecta is >2000 lp/mm at 20% modulation, except at the very edge of the field of view (6-mm radius). This resolution is for a

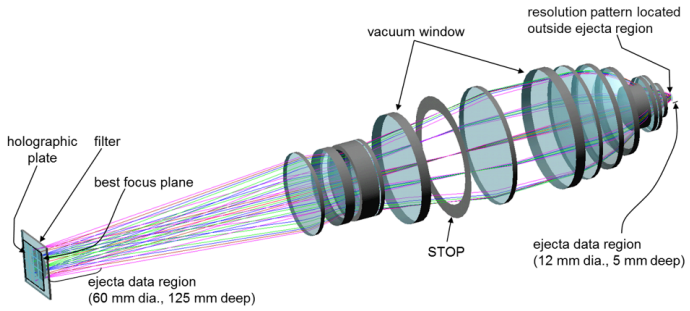

Fig. 2.3.1. Current holographic lens layout.

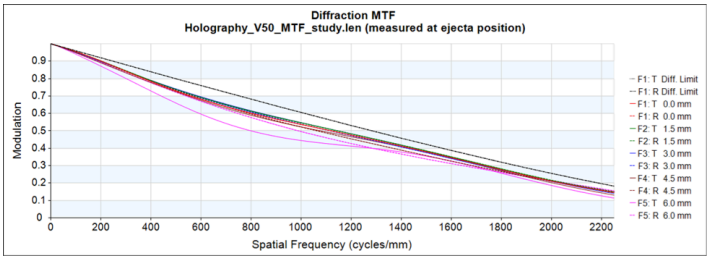

Fig. 2.3.2. Current lens design resolution, as measured at the ejecta position. This position lies along a curved surface.

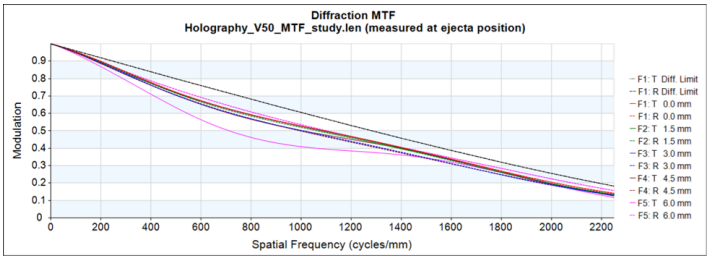

Fig. 2.3.3. Resolution achieved when a flat resolution plate is positioned at the ejecta plane. Some loss of resolution occurs.

curved ejecta surface that has 1330-mm radius of curvature. Careful alignment of the windows and optical elements is required to achieve this resolution. During setup, a flat high-resolution target plate is placed at the grove position. As the lens was designed for a curved ejecta (object) plane, the relayed resolution pattern has some loss of resolution, as seen in Fig. 2.3.3. The figure shows that the resolution has dropped only slightly to about 1900 lp/mm, at 20% modulation.

Another issue with the lens system, is the sensitivity of the resolution to the wavelength. The lens was designed for the tripled YAG laser wavelength of 354.7 nm. Calculations indicate that for a slight change in the wavelength, the resolution is degraded. Figure 2.3.4 shows how, over a range

[c] All previous ejecta measurements using the in-line Fraunhofer holography technique had used a laser with a wavelength of 532 nm.

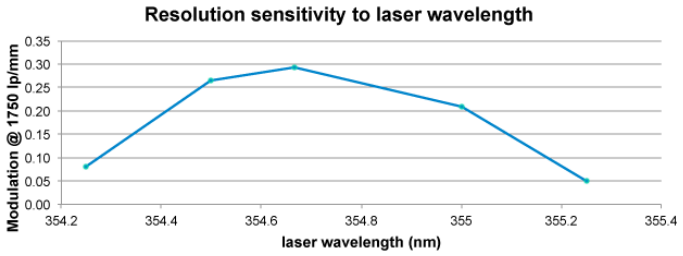

Fig. 2.3.4. Resolution sensitivity to laser wavelength.

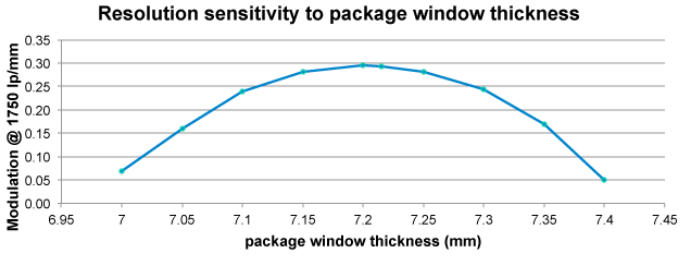

Fig. 2.3.5. Resolution sensitivity to package window thickness.

of 1 nm, the modulation changes from a high of 30% (this result is the modulation at 1700 lp/mm) to a low of 5%.

The lens design also included the three windows that are required for both protecting the lens system and a window associated with the physics package. Figure 2.3.1 and 2.3.7 shows these three windows at the right side of the figure. These flat surfaces produce spherical aberrations and the lens design compensates for these aberrations. Unfortunately, the resolution of the lens system is very sensitive to the glass window thicknesses change. Figure 2.3.5 shows how the modulation changes as the thickness of the package window changes.[d]

2.3.1 Changes made to the Original Lens System

The original lens system is shown in Fig. 2.3.6. With this design, the lens closest to the physics package (labeled 12 in the figure), was fracturing on some of the earlier experiments. Because of this, the lens system was redesigned. In addition, other aspects of how the experiments were setup were changed to help mitigate both shock and fragments that could potentially damage the lens system. Some of these details were mentioned in the previous section. The lens element 12 (indicated in Fig. 2.3.6) was redesigned with the following changes. First, the fabrication of the lens was changed so that both the machining and how the glass was cast were changed to minimize any stresses that might build up in the material. In addition, the glass material was changed as well. In this case, the glass material used for the new lens element was much harder (Knopp-hardness = 410 kg/mm^2) than Ohara PBM18Y glass. After many design iterations were performed, the Ohara glass material S-LAM60 (Knopp-hardness= 730 kg/mm^2)[e] was chosen. It transmits very well at 355 nm, and the lens has a higher index that allows the lens to be thinner, providing an additional 1.5-mm more clearance between the lens

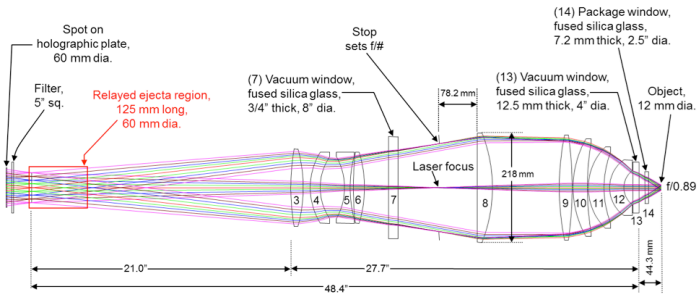

Fig. 2.3.6. Original holographic lens design for recording with 354.7 nm laser light uses nine lenses, providing 5X magnification. Laser light goes from right to left.

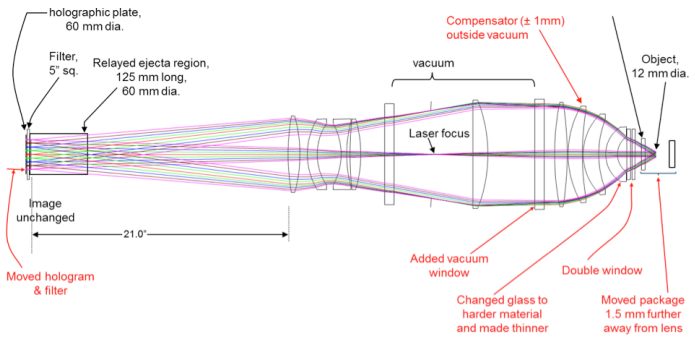

Fig. 2.3.7. Modifications made to the original lens. Moving the package 1.5-mm further away from the lens allowed for more shock mitigation materials to be inserted inside the Boom Box.

housing and the package under test. This extra 1.5-mm air spacing allowed for insertion of rubber spacers between the physics package and the lens flange for shock mitigation as discussed in the previous section. The L12 lens was made to "float" inside its metal mount so no glass material was in contact with any metal hardware.

[d] If the seed laser wavelength were to be slightly different than 354.7 nm, it turns out this can be easily compensated by changing the thickness of one of the windows.

[e] For reference, fused silica has a Knoop-hardness of 500 kb/mm^2.

Another change to the lens system was to move the compensator lens (L10) outside the vacuum. This move eliminated the vacuum seals for the micrometers used to adjust the lens decenter, simplifying the operation. In addition, the original blast window (which also served as a vacuum window) was replaced with a doublet window. Details of the front end of the lens system changes were discussed in the previous section.

2.3.2 Alignment of the lens system

Before the lens can be used in a dynamic event, its alignment and resolution must be certified. The lens is set up at a remote location to the Boom Box. There, counter propagating laser beams (one red and one green) establish an optical axis that allow for display of retro-reflections from the lens and window surfaces. A resolution pattern, made up of arrays of sequences of different diameter dots (and squares), is placed at the ejecta position and a camera records its relayed image close to where the hologram is located. A third UV laser (collinear to the other two alignment lasers) is used to illuminate the resolution patterns that display as patterns with diffraction rings around each dot (and squares). To reduce laser speckle, a spinning plastic diffuser and a static holographic diffuser are used to make the background in the image uniform. The quad group of lenses L3, L4, L5, and L6 can be tilted and decentered relative to the optical axis. The lens L10 can be decentered relative to the optical axis. Both are adjusted to optimize the resolution of the lens system. Archive images are recorded of the diffraction patterns around the resolution dots. Alignment is good when the diffraction patterns are symmetric as the camera moves in and out of focus. The camera has a small FOV, so this operation has to be checked at other positions within the image in order to assure the resolution is optimized through the full FOV of the lens system. A good indication that diffraction limited performance is achieved is to observe color reversal of the resolution dots when the camera moves in and out of focus.

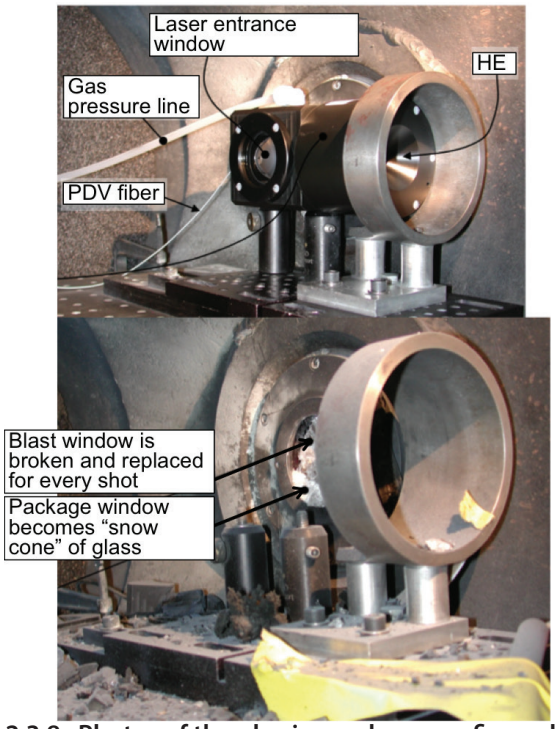

Fig. 2.3.8. Photos of the physics package configured inside the vessel before the expeirment (top) and after the experiment (bottom). The redesign of the lens allowed for insertion of the stainless-Steel barrier to absorb some of the energy

2.3.3 Conducting Dynamic Testing

Two grams of HE does a considerable amount of damage, as shown in Fig. 2.3.8. The top photograph is the experimental physics package just before an experiment, and the bottom photogram is taken just after the experiment. The physics package is primarily made of Delrin, and after the experiment there are many large pieces of Delrin that have fractured. However, as seen in the bottom photograph, the package window has turned into white dust. The outer doublet window protecting the lens, is only slightly damaged. Setting up for a second experiment only requires replacing the outer doublet window, cleaning out the vessel and mounting the new physics pacakge. All this ususally can be accomplished in half a day. The outer window that is replaced has a tilt adjustment built into the front lens flange. This adjustment is done using alignment lasers, and assuring the back reflection from the window is aligned to a reference point determined before the experimental series begins. The new lens system design has proven to work well over the last 25 experiments with no damage to the front lens element (L12).

2.4 SHORT PULSE UV LASER FOR HOLOGRAPHY EXPERIMENTS

A short pulse length Nd:YAG laser, built at LANL and later modified at the STL, has been used successfully for single shot holography of high-speed phenomena, specifically ejecta from experiments at the "Boom Box" facility at the STL. The laser is built on a double-sided 4" thick optical table and surrounded by a light-tight metal housing. On one side of the breadboard, a single pulse from the 80-MHz output of a seed oscillator is selected by a Pockel's cell and directed into a ring, where it is successively amplified by up to seven passes through a flash lamp pumped Nd:YAG rod. After the final pass, the pulse is switched out of the ring by a second Pockel's cell and relayed through a hole to the other side of the optical table where the infrared beam is tripled to 355 nm, then sent through several harmonic separators (to remove 1064-nm and 532-nm light). The 355 nm then passes through a beam expander and vacuum spatial filter (to improve beam quality) and is relayed to the ejecta plane. The 150 ps pulse length and the UV wavelength of the laser allows particles smaller than 1 μm

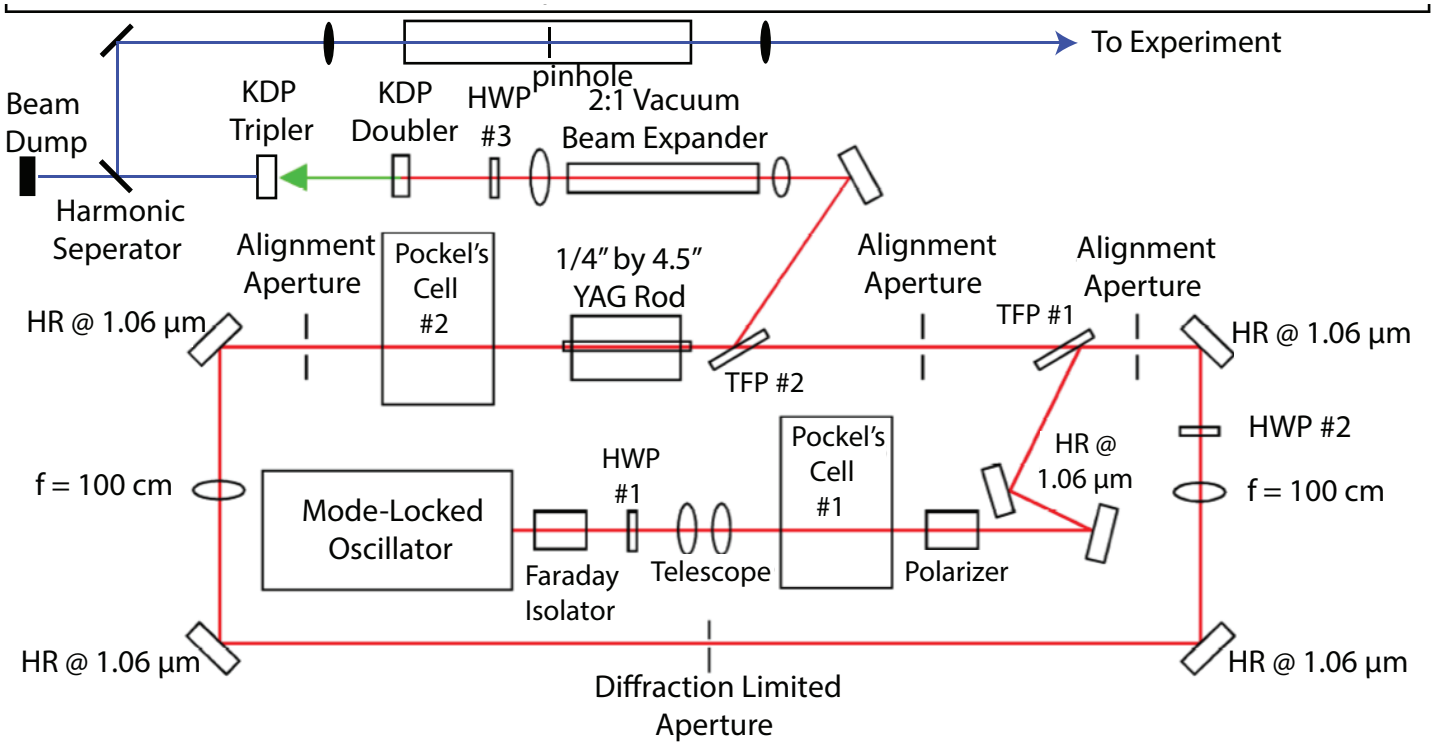

Fig. 2.4.1. Schematic of the high-energy UV laser system used for the holography experiments.

to be imaged at particle speeds of up to 5 mm/µs For these experiments, typical ejecta velocities can range between 2 and 3.5 mm/µsec producing 0.30 and 0.520 µm of blur, respectively. The high-pulse energy (nominally 30 mJ) allows holograms to be taken with standard holography film.

The laser is shown schematically in Fig. 2.4.1. The system is based on a compact mode-locked diode-pumped picosecond laser (Time-Bandwidth Lynx-Van-80MHz-ETL). This is used as the seed oscillator, factory modified by insertion of an etalon to broaden the pulse width to 154 ps and to set the wavelength at 1064.15 nm (wavelength for best pumping of a YAG rod pumped at a low pulse rate). The output of the seed laser, 154 ps, 5 nJ pulses at 80 MHz, is directed through a Faraday isolator and then through a half-wave plate for polarization rotation. Referring to the figue, the beam is directed through Pockel's cell #1 (PC1) and a polarizer, which are used in a fashion similar to a Q-switch to select a single pulse for amplification and output. PC1 must be energized to allow the single pulse to pass. The single pulse is reflected off two plane mirrors and injected into the ring by means of reflection off a thin film polarizer (TFP).

A 0.25 x 4 in. Nd:YAG rod mounted in a diffuse pump cavity (Marysol 1610) is used as the active element in a ring multi-pass amplifier, in conjunction with two Pockel's cells (FastPulse Technology, Lasermetrics Division, model 5046E). One of these cells is used to select a single pulse from the 80-MHz train of the seed oscillator, and the other is used to extract the amplified pulse from the ring. The flashlamp is driven by a rack-mounted flashlamp driver (Analog Modules model 8800), and the laser head is cooled by a closed-circuit recirculating chiller (Thermo NESLAB Merlin M-25). Sending a pulse multiple times through the same medium depletes (saturates) the gain at the center of the beam and flattens the initial Gaussian intensity profile into the flat-top profile desirable for uniform illumination for holography experiments. In addition, gain saturation in this laser helps suppress spontaneous emission. The single amplified 1064-nm pulse, once ejected from the ring cavity, passes through a hole in the "floor" of the two-sided optical table and onto the other side of the table. At this point, the 1064-nm pulse is prepared (diameter and polarization) for tripling by two lenses and a half-wave plate; the two lenses optimize beam diameter and form an image of the amplifier rod output at a point between the doubling and tripling crystals. A vacuum tube between them (kept ≤ 100 mTorr by pumping as necessary) prevents air breakdown by the intermediate beam focus. On passing through the first crystal, a temperature-stabilized KDP crystal, much of the beam energy is converted to 532 nm. Immediately following this "doubler" is another KDP crystal, a "tripler," which takes some of the 532-nm light and the remaining unconverted

1064-nm light and outputs 355-nm light. Because of the nature of doubling and tripling, the temporal width of this 355-nm pulse will be slightly shorter than the initial 154-ps pulse at 1064 nm. Furthermore, the beam will contain significant amounts of unconverted 1064-nm and 532-nm light, so the beam is subsequently passed through a number of harmonic separators, (mirrors that reflect 355 nm and allow the other two wavelengths to pass through to a beam dump) for spectral cleanup. Following cleanup, the 355-nm beam passes through a two lens beam expander (f = +1000 mm and f = +2036 mm) that produces a very slightly diverging beam with a magnified image of the amplifier rod at the object plane of the hologram (note that in this laser's image relay system, an image was also formed between the doubling and tripling crystal). Laser-beam diameter at the ejecta plane in the vessel is 18 mm, and the distance from the final lens in the laser to this object plane is approximately 2350 mm. A vacuum tube was originally located between the two lenses to prevent air breakdown. It was later modified to be a vacuum spatial filter by the addition of a 600-micron pinhole at the focus of the f = 1000 mm lens; this modification resulted in a significant reduction of unwanted structure in the final output.

2.5 Holography Reconstruction System and Analysis

2.5.1 Analysis

The analysis of the hologram flows through three steps. These steps are, in order: the scanning of the hologram with the blue light reconstruction bench, executing the preliminary analysis, and finalizing the analysis.

Fig. 2.5.1. Photograph of holography reconstruction bench here the image volume is reconstructed and converted into digital images.

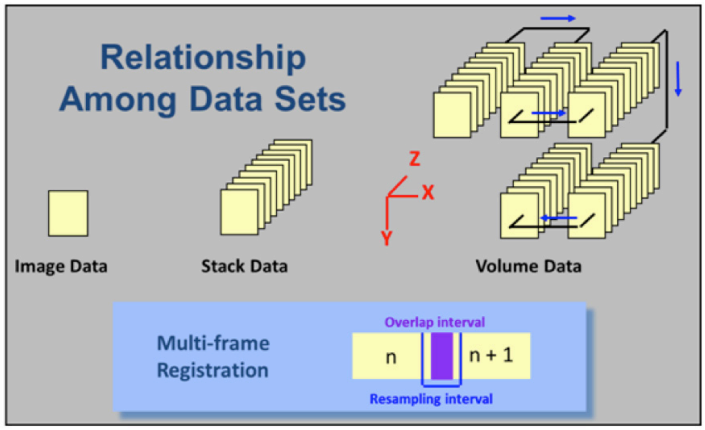

Fig. 2.5.2. A schematic of how the image volume is scanned with the camera system.

2.5.2 Blue Light Reconstruction Bench

The photograph in Fig. 2.5.1 shows the blue-light holographic reconstruction bench with the (A) laser at the far left, which operates in continuous wave mode at 354.67 nm. Relative to the hologram, the laser is aligned in the same direction as the laser was aligned when the hologram was produced. This 354.67 nm laser light propagates through the (B) UV beam expander and onto the (C) UV collimating lens. The collimated light then illuminates the (D) hologram as it rests in the three axis stages. Light passing through the hologram then passes through the (E) relay lens and then to the (F) camera at the far right, where the image data are acquired. These image data are acquired as the stages move the hologram through a programmed sequence of positions.

The (G) joy stick, (H) three axis controller, (I) display monitor, and (J) computer monitor are part of the computer control system that is used to program and execute programmed scans of the hologram. Figure 2.5.2 summarizes the structure of the scanned data. First, the orientation is defined by the three axes in the center of Fig. 2.5.2. The z axis is along the direction of the laser beam. For the data in this report and in terms of the scanned data, the ejecta are moving from left to right along the x axis. As the stages move the hologram through its set of programmed positions, the image data are acquired. The stages first step along the z axis in the direction of the laser beam at programmed increments. With each step, the camera acquires an image, names the image according to the scan name and image number, and saves the image data. These image data are thus named in the order in which the data were acquired. The image data that are acquired at the same x and y motor coordinates but at different z motor coordinates are referred to as stack data. The top of the stack refers to data that were acquired furthest away from the camera while the bottom of the stack refers to data that were acquired nearest

to the camera. At the end of each stack, the motors step the stages to a new x and y setting, beginning with x first. In each of these x and y steps, the system allows for some overlap between the images for registration. Then, against the direction of the previous stack, the system again scans data along the z axis. When the motors reach the end of the scan in the x direction, the scan position is stepped in y. The process repeats itself with the motors now stepping the back toward the original x position location with each new stack. When the scan reaches the original x position, the motors then step the hologram to next y position. The scanning and reversals continue until completion. The ordered data set within a stack now describes a volume. This volume data can be characterized as number of frames per row, frames per column, and frames per stack. Most scans in this report consisted of four frames per row, 20 frames per column, and 160–200+ frames per stack. For example, a typcial scan of 4×20×160 frames gives 13000 images that are analyzed. Overlap between frames was 5% with five micron steps along the z axis. Pixel dimensions relative to the experiment space was 0.250 micron per pixel. When the data are processed, background data are estimated for each stack. While this background estimate will be different for each stack, the entire scan is processed as one dataset.

2.5.3 Preliminary Analysis

The preliminary analysis performs two separate passes to extract anomalous data. The first pass extracts anomalous data based on intensity thresh-holding. This intensity thresh-holding will extract some of the larger, and medium sized particles and most of the smaller particles. The second pass extracts particles based on the sharpness of intensity profiles. Particles that are extracted during the second pass will tend to be the smaller particles.

To locate anomalous data during the first pass, the preliminary analysis begins by using a background image to compute the signal excess for each image in the stack by subtracting the background from each image in the stack. The maximum difference at each pixel is retained as the maximum signal excess, *MaxS*. This maximum signal excess will always have non-negative values although some differences may be negative. These image data are raised to the fourth power to construct a weighting function, *MaxI*.

The analysis also divides the image data into a number of zones based on the background image. From the *MaxS* values, the analysis computes an initial threshold for each background from a weighted average of the maximum signal excess, *maxS*. The weights come from the *MaxI* image as

$$MaxBT(k) = \frac{\sum MaxI(i,j) * MaxS(i,j)}{\sum MaxI(i,j)}$$

where the (i,j) is the set of all points belonging to the zone k.

Next, a lower weighted threshold is computed using only the set of points (i',j') within the zone k that have maximum signal threshold levels less than $MaxBT(k)$. This lower threshold is

$$MaxBT(k) = \frac{\sum MaxI(i',j') * MaxS(i',j')}{\sum MaxI(i',j')}$$

From this point, a set of rules compares the zones, the background levels that they represent and their respective $MaxBT(k)$ and $MinBT(k)$ values to set the final threshold value. The *MaxS* values are compared against the final thresholds and points where the *MaxS* values equal or exceed these thresholds are extracted as potential particle data.

For the second pass extraction, the analysis computes a sharpness feature for the data. A sharpness threshold is determined from the sharpness features from the first pass particle extractions. Only edge pixels (particle pixels that are adjacent to non particle pixels) are used to determine this threshold. All the first pass particles are subjected to this threshold. First pass particles that do have edge pixels that exceed this threshold are rejected. The sharpness feature for all other data that did not satisfy the first pass intensity threshold are then subjected to this sharpness threshold. The second pass particles are then extracted where this sharpness threshold is satisfied. The first pass and second pass particles are then combined. Their centroids are computed and they are fit to a rotated ellipsoid to calculate major and minor axis as well as angle of rotation. The output data set lists particles by number, stack number, area, centroids, and major and minor axis and angle of rotation.

2.5.4 Final Analysis

The preliminary analysis segments data on the basis of the maximum signal intensity and derives depth information accordingly. This approach may be valid for the smallest particles. During the reconstruction, these smallest particles will come into focus over a very limited number of frames as data are acquired along the laser axis. However, the largest particles may appear to come into focus more than once. The apparent focus zones may last for several frames. In such cases, the behavior of the reconstruction will be different each of the zones. In one zone, the reconstructed particle may appear to be very bright and smaller than the true area. In another zone, the particle may appear larger but less bright. For these largest particles, errors will be generated relying only on the maximum signal intensity. The final analysis constructs a rectangular volume of interest (VOI).

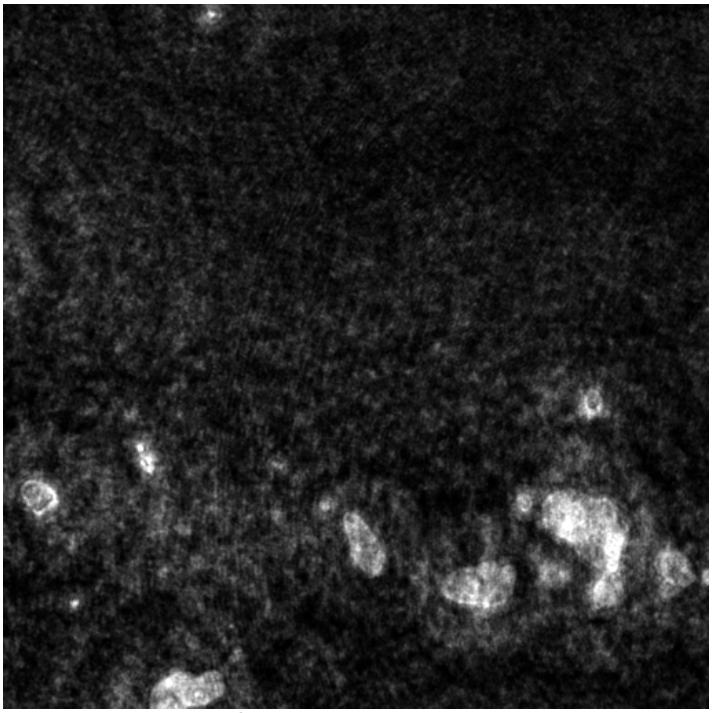

Fig. 2.5.3. Raw data frame E09BC2640 raw.

The face (x- and y- extents) of the VOI is determined by the maximum x- and y-extents of the particle plus a 2.5-micron buffer. The length (extent along the laser axis) is determined by the area of the particle. This VOI is centered about the x-, y-, and z- coordinates that were extracted for the particle. The z locations within the VOI actually correspond to a particular frame number in the scan. At each z location, the analysis extracts a region of interest (ROI) of the raw data from that particular frame number. This ROI is centered about the x- and y- image coordinates of the particle. The analysis then determines a threshold intensity that is the nominal midpoint intensity of the background and maximum particle intensity to segment the particle. Additional operations are applied to smooth the edges of the particle and to fill in voids.

An important consideration for this approach to the analysis is that the analysis will determine a threshold and will extract a particle even when no particle actually exists. This erroneous extraction can occur when the derived threshold is too low to be realistic of a particle. The analysis needs to compute a "goodness" factor. The goodness factor evaluates the segmentation as either good with a value of one or bad with a value of zero. Other features calculated for the particle include an effective area and a sharpness factor. The best solution is determined from the maximum product of the effective area and sharpness factor where the goodness factor is one. A final step in the analysis registers the extracted data and removes particles that are multiply counted tallies the 3D coordinates of the particle, and the corresponding properties of the particle such as the area of the particle that is used to calculate the particle diameter. and computes the particle size histograms. An example of the result of the analysis of one stack of data is shown in shown in Fig. 2.5.4. A raw image plane acquired from reconstructing the hologram is shown in Fig. 2.5.3, which shows some of the particles in focus. The raw image is near the central plane for this stack of 161 frames. The bright areas are the particles. Because the analysis results are for the entire stack, the single image comparison will not correlate exactly with the summary analysis in Fig. 2.5.4.

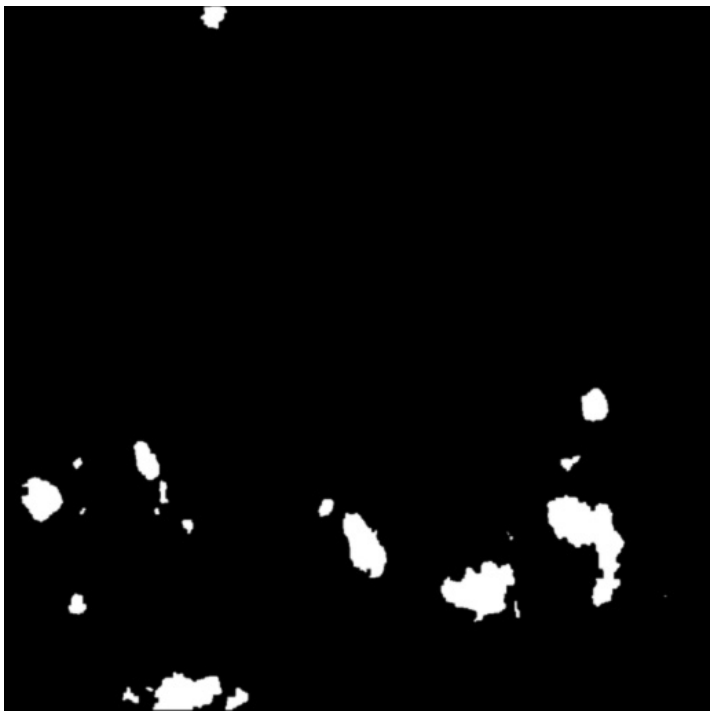

Fig. 2.5.4. Result of the analysis of one of the stacks of image data from which Fig 2.5.4 is one of the frames.

3. EXPERIMENTAL RESULTS.

In Section 2 of the report ,the physics package was described in some detail. For all the results described in this report, a 2-mm-thick, 40-mm-diameter Sn target was used. The Sn was diamond turned on both sides and a 40-micron deep groove is machined 1.0 mm from the center of the target. The opening angle of the groove is 120 degrees, and the width of the groove at the surface is 140 microns. The shock wave in the Sn is generated using 12.7-mm-diameter, 12.7-mm-thick 9501 high explosive. This configuration gives rise to a shock pressure near 300 kbar at the free surface, which is above melt-on-release. The resulting microsheet provides the initial conditions for ejecta production.

A problem encountered with previous holography measurements was the limitation in which only the fastest moving ejecta could effectively be measured. This limitation exists because the density of particles was too high to allow enough unscattered light through the ejecta volume to form the interference patterns on the holographic film. In

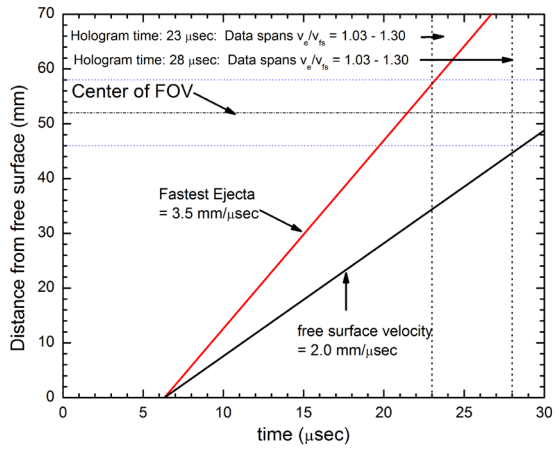

Fig. 3.0.1. Trajectories of the free surface and the fastest moving ejecta (shown in red). The two times 23 and 28 micro-seconds are indicated as the vertical dotted lines. These two times allow the full velocity distribuiton to be obtained as seen in the figure.

addition, multiple scattering also becomes a problem when the ejecta particles density is too great. Two experimental design features were carried out to deal with the potentially large amounts of ejecta. The first was to use a single groove to generate a thin sheet of ejecta. The second was to locate the field of view high above the free surface to allow more time for the ejecta particles to spread out in space. In Fig. 2.2.4, the center of the FOV is shown which is located at a distance of 52 mm above the free surface.

Figure 3.0.1 shows the target free surface position and the position of the fastest moving ejecta particles vs time. The fastest moving ejecta are primarily determined by the groove angle. In this case, the fastest moving ejecta has an ejecta velocity (v_e) of 3.42 mm/μsec or 1.7 × free surface velocity (V_{fs}). In order to capture the full velocity distribution, two separate experiments were conducted at 23 μsec, and 28 μsec. These two times are indicated in the figure as dotted vertical lines. Also shown in the figure are two horizontal lines indicating the 12-mm diameter FOV for the holography measurement. The two experiments at 28 and 23 μsec cover the velocity ranges of v_e/v_{fs} = 1.03 – 1.34 and 1.34 – 1.69, respectively. As the effective FOV is larger than indicated in the figure, the velocity range is somewhat larger allowing for an overlap in the velocity range for the separate experiments. The data from the overlap regions can be compared as a check that the production and fragmentation of the microsheets is similar in both experiments.

3.1 Results from Vacuum experiments

In this section, results from two experiments conducted in a vacuum environment will be presented. Some details of these experiments are indicated in the first two rows of Table I. As mentioned above, the experiments are hydrodynamically very similar as evidenced by the fact the free surface velocity measurements were essentially the same as indicated in the table. All the data presented in this report use targets that have the same precision groove machined into the surface. The angle of the groove is determined by the machine tool, which is 120 degrees. Appendix 1 shows the free surface velocity for one of the experiments.

3.1.1 Three Stages of Breakup

For these experiments, it was observed that the microsheet breaks up into particles in three stages. Figure 3.1.1 shows a high-resolution shadowgram of the microsheet, which is moving from left to right. The timing of the image was such that the free surface is just to the left of the image. The horizontal axis is the position above the static free surface, so that 46 mm is very close to the dynamic free surface. The upper horizontal axis is (v_e/v_{fs}). 00In this case, the free surface velocity is 2.0 mm/μsec. At the top of the image is a calibration wire located at 58.0 mm above the static free surface. The black parts of the image are the Sn material. Clearly, near the free surface, the material has not completely broken up and well-defined closed structures are observed as indicated by the arrow. Looking further to the right these closed structures are no longer evident, and the structures are predominantly tendril-like in nature. Finally, above about v_e/v_{fs} = 1.1 most of the Sn material has fragmented into well-defined particles. For these velocities and higher, particle-size distributions can be obtained. From

Table I: Caption

Experiment #	Date	Pressure (psia)	Holography time (μsec)	V_{fs} (mm/μsec)
Shot 1	February 10, 2014	Vacuum	28.0	2.004
Shot 2	July 18, 2013	Vacuum	23.0	1.944
Shot 6	February 13, 2014	5.7	23.0	2.028
Shot 5	February 12, 2014	12.0	23.0	2.031
Shot 4	February 12, 2014	15.1	23.0	2.007
Shot 3	February 11, 2014	19.0	23.0	1.995

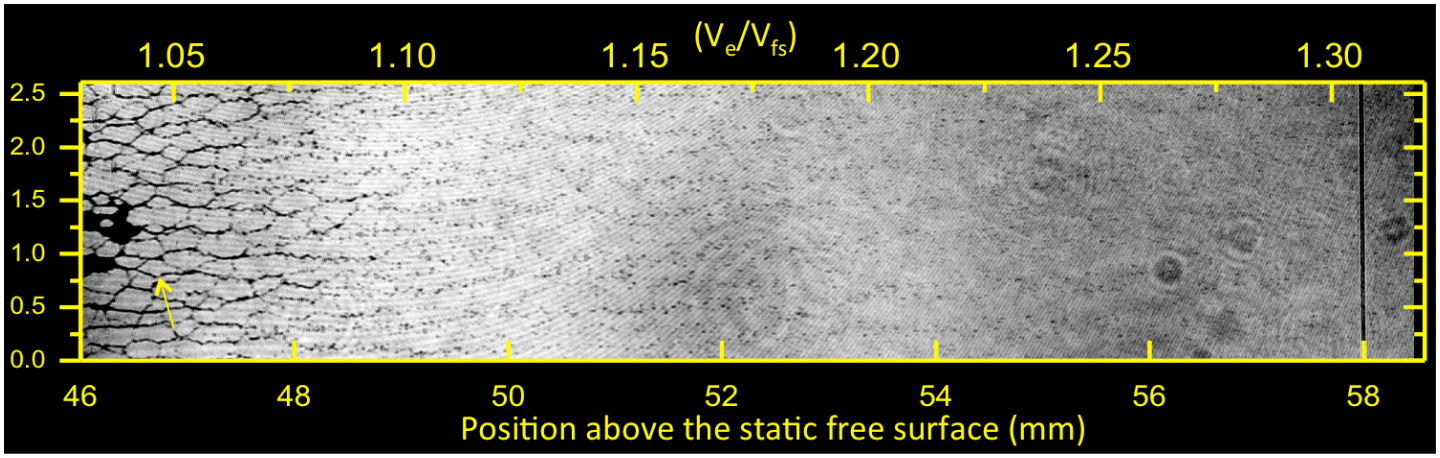

Fig. 3.1.1. Zoomed region of the late time hologram clearly showing the web-like structure and tendrils (in black). The free surface is located just to the left of the image. The lower horizontal axis is position above the static free surface, and the vertical horizontal axis is v_e/v_{fs}. The 10 micron wire is shown at the far right at 58 mm above the free surface.

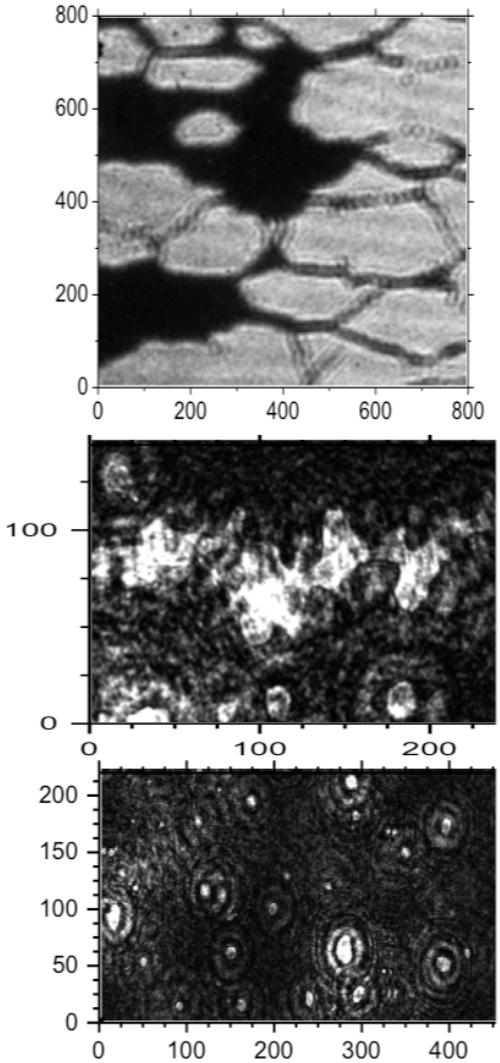

Fig. 3.1.2. Illustration of the three stages of microsheet breakup. The top figure shows the stage at which the microsheet is in both solid sheet and web-like state. The middle image shows a long tendril in the middle of the image surrounded by a few well-defined particles. The bottom shows the last stage where all the ejecta exist as well-defined particles.

this detailed image three stages of microsheet breakup are observed and can be described as follows:

1. Solid sheets breaking up into closed web-like structures
2. Closed web-like structures breakup into tendrils
3. Tendrils breakup into particles

These three stages are illustrated in Fig. 3. 1.2. The top image shows a shadowgram, and the second and third images are reconstructed images obtained from the hologram. For these last two images, the particles are shown as white structures, which are reversed from the shadowgram image. Both x and y axes are in units of microns. In the top image, which is very close to the free surface, the web-like structures are clearly evident. Also shown in this image are a few solid sections of the microsheet that have not yet transitioned into the web-like structures. The thickness of the strands from the image is about 25 μm. The second image shows one tendril that resulted from the breakup of the web-like structure. Also seen in the image are a few well-defined particles. This image corresponds to v_e/v_{fs} = 1.03. Finally, the last image shows well-defined ejecta particles with v_e/v_{fs} = 1.1. For all regions above this velocity range, particles are observed and particle size distributions can be obtained.

3.1.2 Ejecta Particle-Size Distributions for Different Ejecta Velocities.

Particle-size distributions from the analysis of two experiments will be presented in this section. Figure 3.1.3 shows the two shadowgrams of the two experiments at 28 and 23 μsec respectively. In the figure, the ejecta is moving from left to right. For the shadowgram on the left side of the figure, the free surface is located just to the left of the image. The black web like structure can be observed in the left side

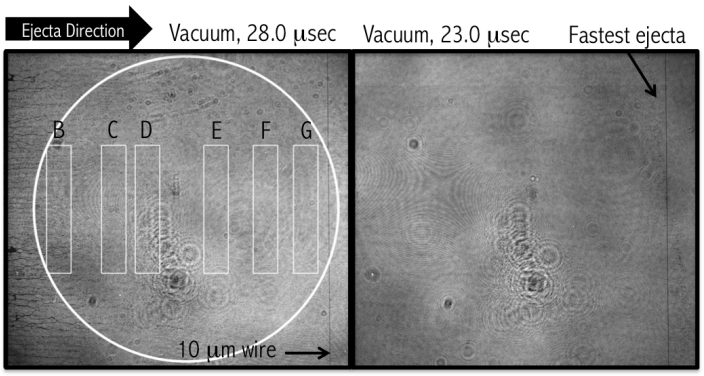

Fig. 3.1.3. Two images of the holograms (shadowgrams) used for the present vacuum analysis. The image on the left was acquired at 28 μsec, and the image on the right was acquired at 23 μsec essentially capturing ejecta at all velocities. The white circle indicates the nominal FOV for the holograpy measurement, and the rectangular regions labeled B - G are the regions analyzed in this report

of the figure. Not so clear from the figure is the fact that ejecta particles are present everywhere on the hologram. The figure on the right side is the hologram acquired at 23 μsec, at which time the fastest moving particles are near the 10-μm wire. The circle shown in the figure is 12.0 mm in diameter. This view is the nominal FOV for the optical relay system. However, data are obtained outside this region with worsening resolution the farther from the circular region the data is analyzed. For the distributions presented here, the rectangular regions (labeled B-G) were scanned and analyzed.

Figure 3.1.4 summarizes the particle-size distributions for the two vacuum experiments in which most of the velocity distribution has been sampled. In order to obtain better statistics, two scan regions[f] have been added and the average velocity obtained. In the top left panel of the figure, the slowest moving ejecta particle-size distribution is shown. This distribution shows an enhanced tail region compared with the other distributions. As the free surface is approached, not only are the particles larger on the average but there exist the tendrils discussed in Section 3.1.1. These large structures have not entirely broken up and flatten the distribution as seen in the figure. Figure 3.1.5 shows an example of one of these regions. The image at the top is a reconstructed raw image from the hologram in a single plane where some of the particles are in focus. The bottom image is the result of the analysis of the stack of raw images as described in Section 2.5. At the bottom of the image a tendril that is ~ 120 μm long is seen. The bottom image indicates the analysis is doing well in extracting these large structures. Referring back to Fig. 3.14 in regions where v_e/v_{fs} are greater than 1.1, tendrils are no longer observed and the particle-size distributions are seen to steepen slightly moving the average particle size to smaller values. Once v_e/v_{fs} reaches approximately 1.3, the distributions change very little. Figure 3.1.6 shows how the average size changes over most of the velocity distribution. The first five points range over values v_e/v_{fs} from 1.08 to 1.27. In this range, the average particle diameter changes from 7 μm to 4.5 μm.

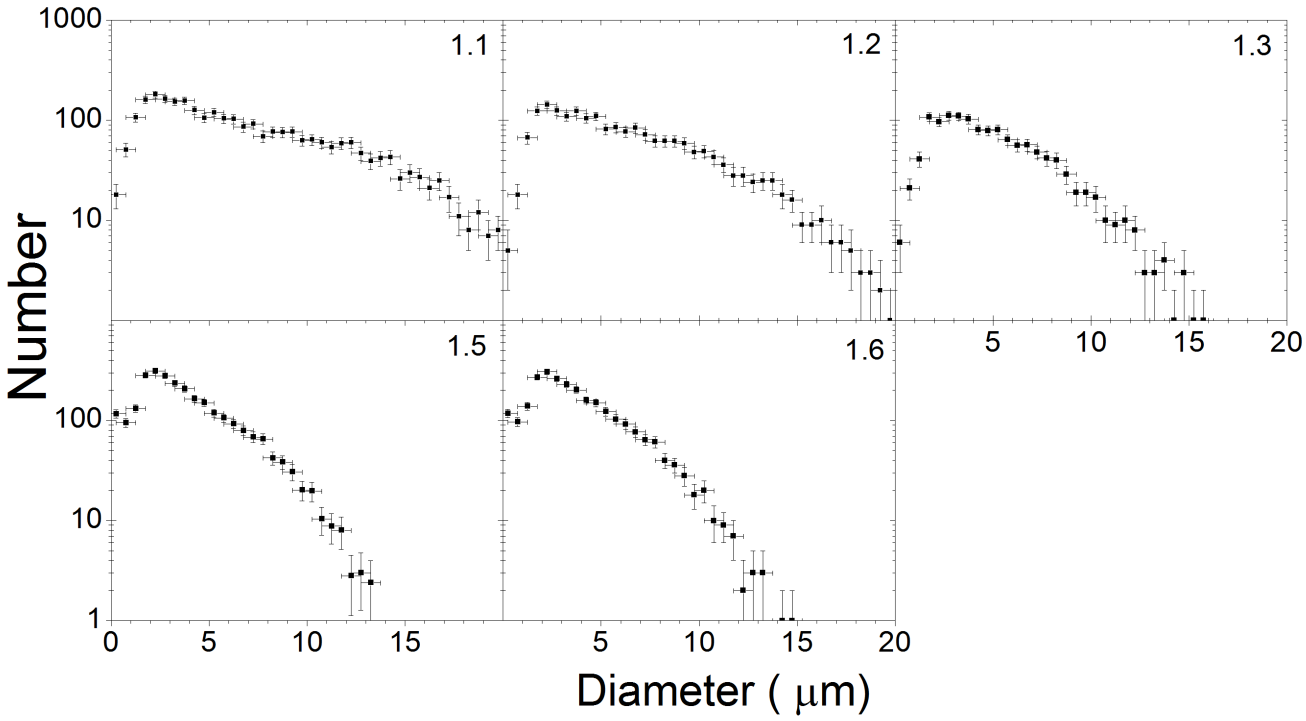

Fig. 3.1.4. Particle-size distributions for different values of v_e/v_{fs}(shown in the upper right hand corner of each panel) The distributions have been averaged over multiple scan regions.

[f] For the last panel at v_e/v_{fs} = 1.6 three regions were averaged.

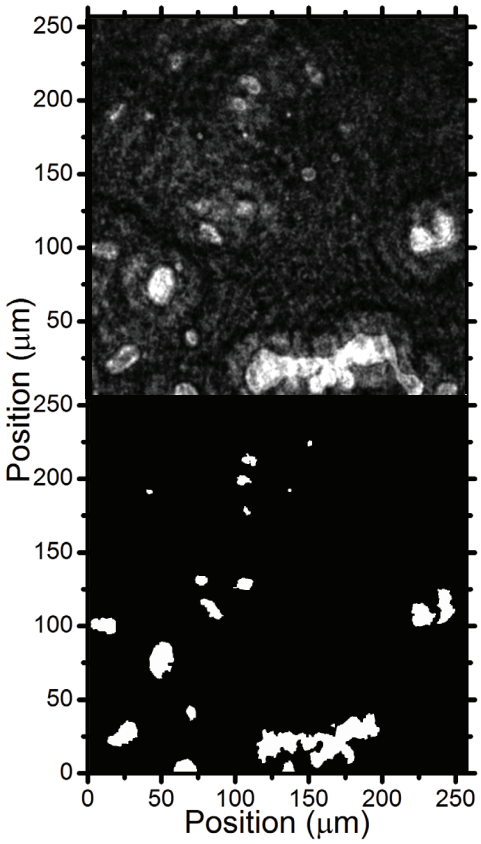

Fig. 3.1.5. Example of one region of ejecta where tendrils still are present. The top image is a raw reconstructed image. The large tendril is shown at the bottom of the image. The corresponding result from the analysis is shown in the bottom panel.

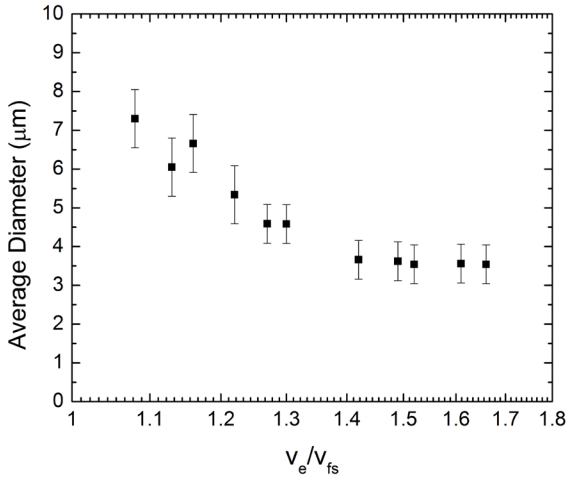

Fig. 3.1.6. The average partice diameter as a function of ejecta velocity.

Beyond v_e/v_{fs}=1.4 the average particle diameter of ~ 3.5 μm changes very little.

3.2 Results from the Gas Experiments

Results from four helium gas experiments will be presented in this section. Some of the details of these experiments are indicated in rows 3–6 in Table 1. The helium gas causes the particles to not only slow down as a result of drag, but from the holography results, it is observed that the gas interacts strongly with the liquid drops, breaking them up into smaller particles. This effect increases as the gas density increases, moving the average size of the distribution to smaller sizes. Unfortunately, it is difficult to obtain high-quality holography results in a gas. It is possible the shock wave in the gas is changing the index of refraction of the gas environment distorting the scattered and unscattered wave fronts. When the hologram is reconstructed, the corresponding images are distorted and noisy. As the gas pressure increases, this effect also increases. Reasonable holography results can be obtained with absolute helium gas pressures up to about 19 psia. Shadowgrams of the four experiments are shown in Fig 3.2.1. The top panel has the smallest gas pressure of 5 psia. This pressure is very near to vacuum pressure levels used for the vacuum experiments. The approximate location of the leading edge of the ejecta is indicated by the yellow arrows. The 10-micron wire is seen at the right side of the image. The ejecta is moving from left to right. As the pressure of the helium gas in-

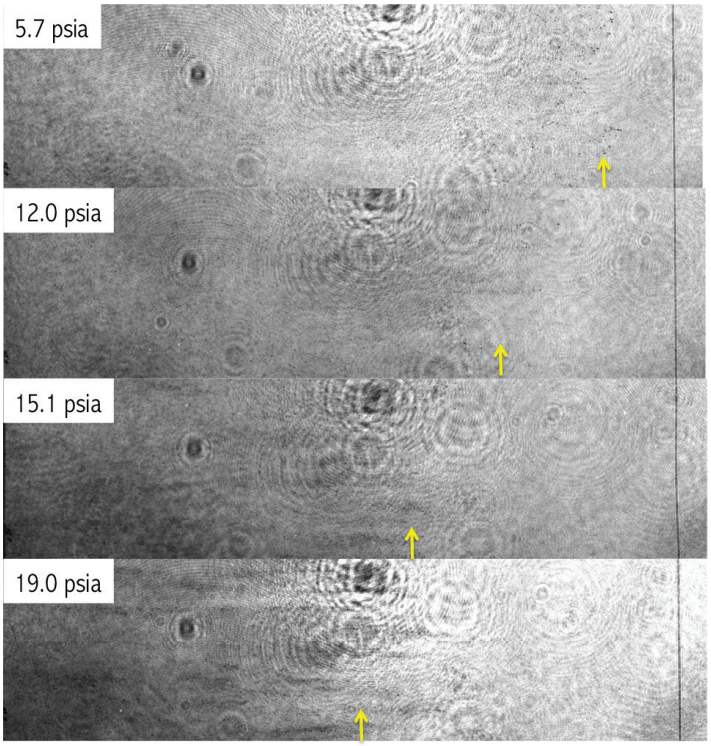

Fig. 3.2.1. Shadowgram regions obtained from the hologram for the four different gas pressures. The darker region is the ejecta cloud (moving left to right), and the yellow arrows indicates the approximate location of the ejecta front.

creases, the leading edge of the ejecta moves to the left as indicated by the yellow arrows. These four experiments were identical except for the gas pressures. Four regions of the holograms were used in the present analysis. Referring back to Fig. 3.1.3, these four regions were B, C, D and E, The regions F and G used for the vacuum analysis, were not used in the analysis of the helium gas data because they reside outside the particle region for some of the larger helium gas pressure experiments. The particle size distributions are summarized in Fig 3.2.2. The lowest gas pressure, which is very near vacuum pressures, show a size distribution similar to the vacuum data. The figure shows that the shape of the distributions becomes steeper for the higher gas pressures, driving the average particle size to lower values. This result is consistent with the picture that the larger particles are breaking up into smaller particles changing the shape of the distribution as described above. These results are summarized in Fig. 3.3.2 where the average particle size is plotted as a function of helium gas pressure. Also shown in the figure as the solid circles are exponents that were found by fitting the tail region of the distribution with a power law. As the distributions become more forward peaked, the slope of the tailing part of the distribution becomes steeper.

3.3 Comparison between Vacuum and Gas Ejecta Particle Size Distributions.

As discussed above, the gas is seen to have a significant effect in breaking liquid particles apart. Even relatively small amounts of gas can interact with the particles in a significant manner. In this section, a comparison is made between particle-size distributions in a vacuum and gas for an average value of v_e/v_{fs} = 1.5.. Figure 3.3.1 shows a comparison between the vacuum distribution and the gas distributions as shown in the previous section. The number distributions are for similar ejecta velocities and the data has been normalized to similar particle volumes. The comparison shows a clear trend as the gas pressures is increased. The larger particles are breaking up and therefore the number of smaller particles increases relative to the larger particles, steepening the slope of the distribution The figure shows the difference between the two distributions.

3.4 Double Pulsed Holography

Recently, the high-powered laser used for the holography experiments was reconfigured so as to produce two pulses

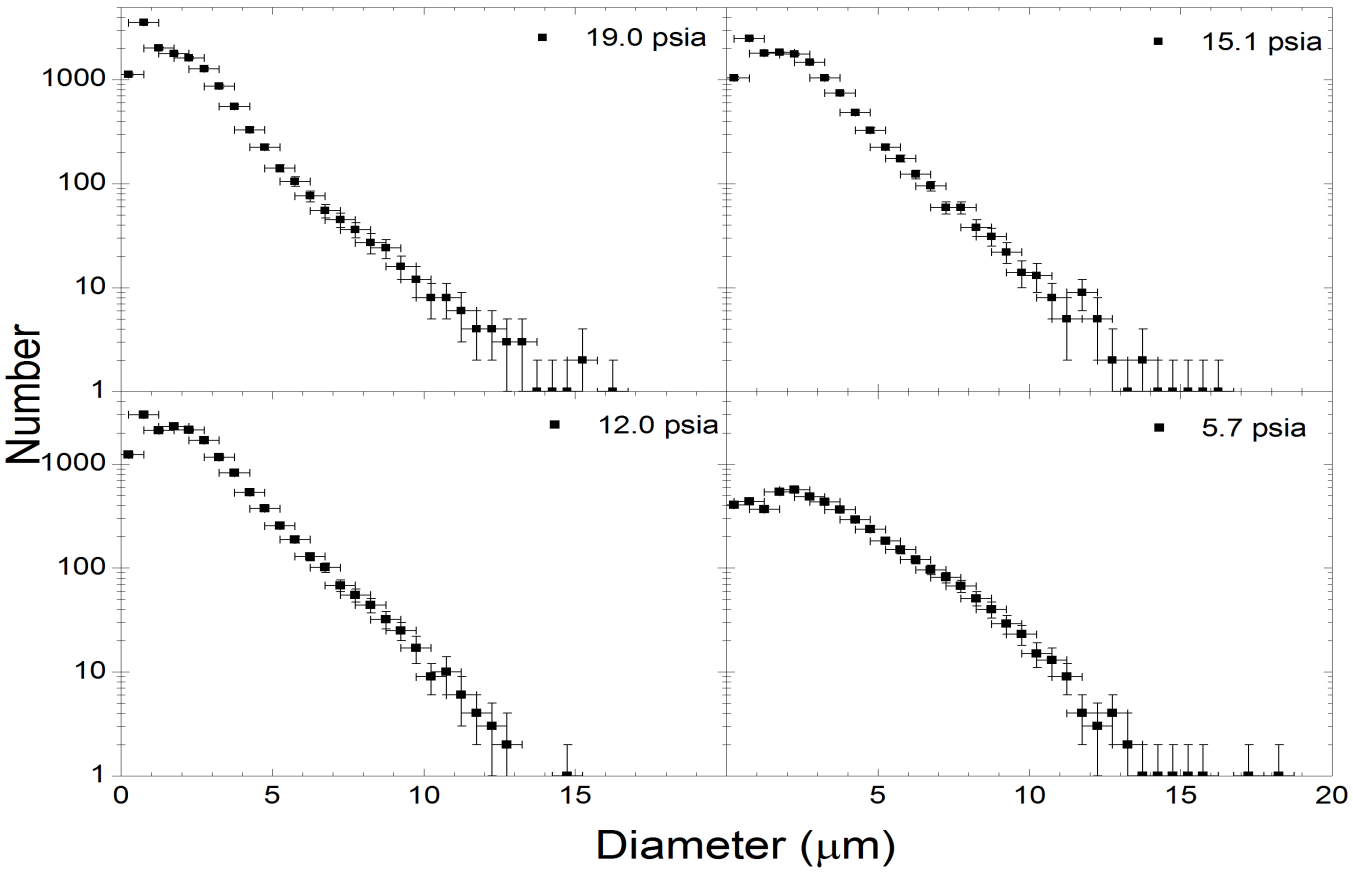

Fig. 3.2.2. Ejecta particle size distributions with an average v_e/v_{fs} of 1.5. The four distributions shown are for four different helium gas pressures ranging from 5.7 psia, (which is very close to pressures used for the vacuum experiment) to the highest pressure data shown in the top right panel of 19.0 psia.

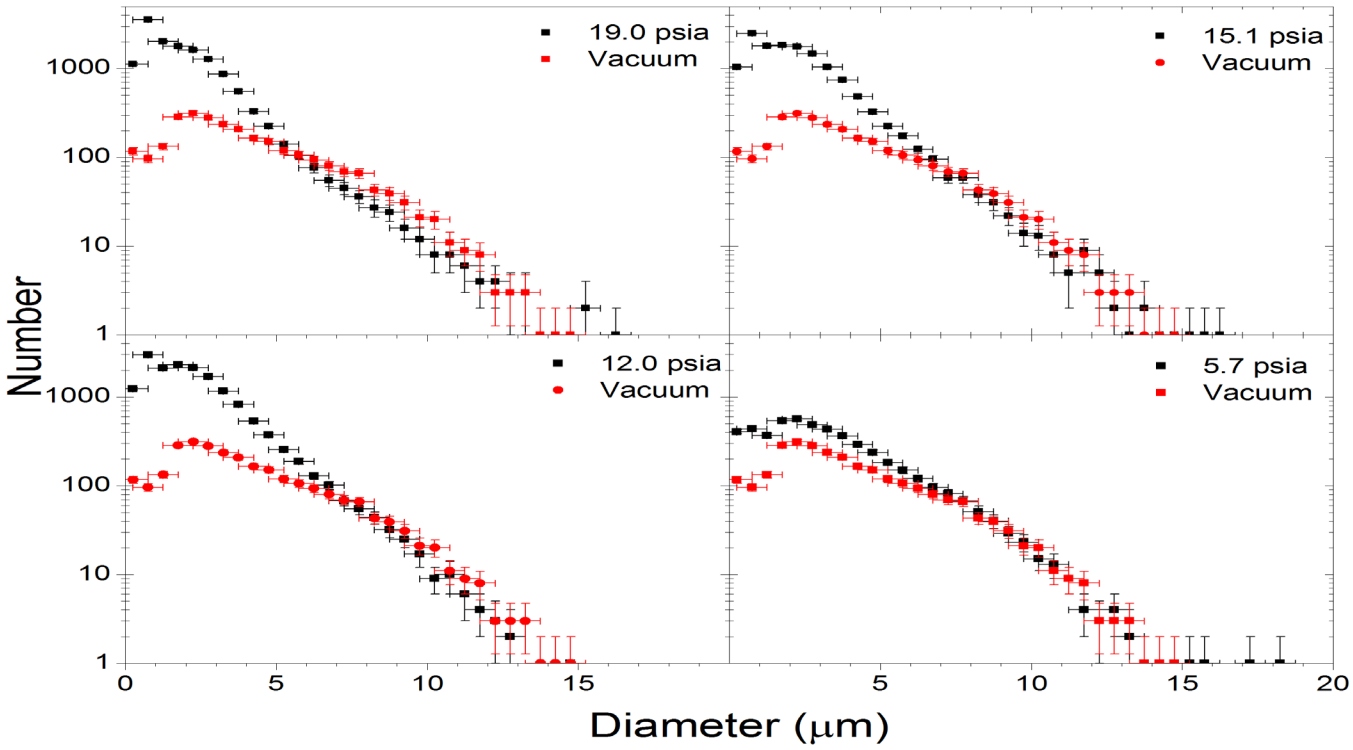

Fig. 3.3.1. Average ejecta particle size distributions in helium gas and Vacuum. The helium gas data is identical to that shown in Fig. 3.2.2. and is for an average v_e/v_{fs} = 1.5

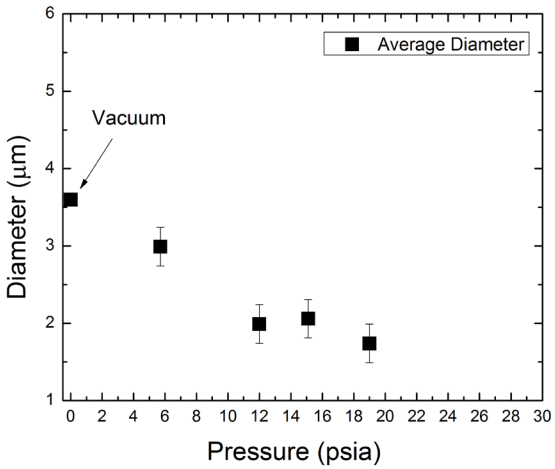

Fig. 3.3.2. The average particle size given by the distributions in Fig. 3.3.1 are shown as the solid black squares.

separated by 6.8 ns. The laser-beam pulse separation was accomplished by using a beam splitter, delaying one of the pulses relative to the other in space by about two meters. The two pulses were recombined and on the same beam axis. In this configuration, two holograms were recorded on one piece of film. During the reconstruction, the particle fields at both times were superimposed on one another. An example of one of the reconstructed regions is shown in Fig. 3.4.1. The image clearly shows particle doublets. The velocity is from left to right and the doubles are predominantly along the horizontal axis indicating the velocity is in one direction. This indication is as expected for ejecta launched into a vacuum. These double-pulsed data allow the ejecta velocity distributions to be measured directly by simply measuring the distance between the two particles and dividing by the time separation (in this case 6.8 ns). For many of these types of experiments, it is usually assumed that all ejecta particles are produced at the free surface jump-off time and have a velocity perpendicular to the free surface. With the double pulse data, this assumption can be checked very easily by plotting the measured vs. expected velocities. The result is shown in Fig. 3.4.2. The correlation is not perfect. For a perfect correlation, a slope of 1.00 would be obtained. However, a fit to the data gives a slope of 1.07 indicating the ejecta particles are moving slightly slower than predicted.

4. FUTURE WORK:

The UV in-line Fraunhofer holography diagnostic described provides a unique set of data in characterizing ejecta particles size, shape and position. The improvements to the diagnostic and the ability to carry out numerous experiments in a cost effective manner, allow various aspects of

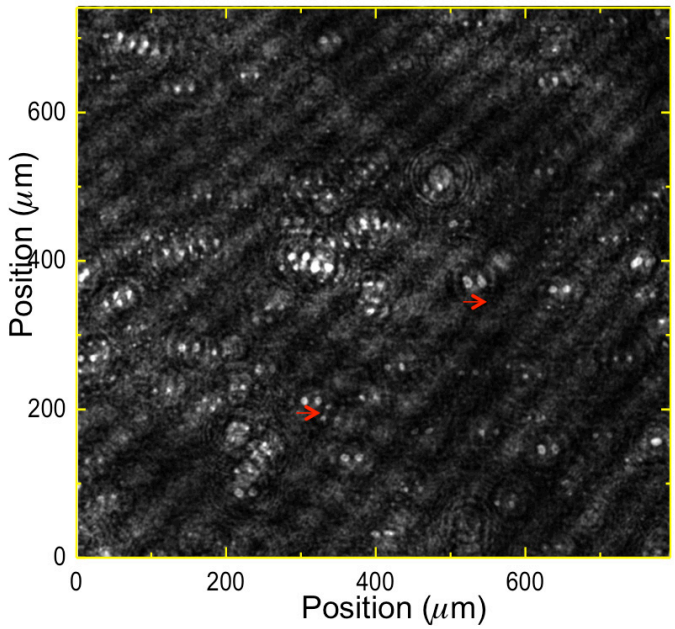

Fig. 3.4.1. Mosaic of raw image data where many of the particles are in focus. The pairs of particles are easly discernabe. The red arrows indicate the direction of the ejecta particles.

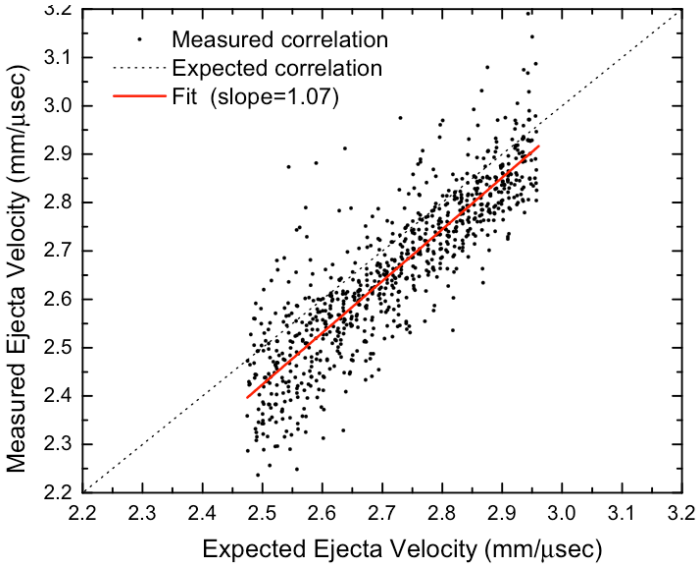

Fig. 3.4.2. A region of the hologram is analyzed and the expected velocites are plotted agains the measured velocities.

ejecta physics to be explored systematically. Currently, a rich set of data has been obtained in both vacuum and helium gas environments and the analysis of this data is ongoing. In particular, the physics of liquid particle breakup in a gaseous envirmontment is currently being investigated with particle size distribution being obtained for different helium gas pressures. Three areas in particular are planned for future work:

1.) The physics of gas interaction with liquid particles will be a continued focus. A limited set of data has been analyzed and presented here, However, more data can be extracted from the holograms, and will be analyzed for future work. In addtion, the helium gas data obtained thus far did not sample the full ejecta velocity distributions. Another holography experimental campaign is planned for fiscal year 2015 in which late time data will be obtained so that a complete velocity range will be covered. This will also allow a more direct and useful comparison with the vacuum data. Finally, as the quality of the data has been observed to be degraded with increasing helium gas pressures, a physics package design modification will be studied to determine if the noise can be reduced.

2.) Data from a variety of groove geometries have been obtained. This data will be analyzed to determine if any identifying trends in the data can be observed that would allow a model to be developed that could predict the size distribution based on the initial groove geometry. Parameters such as the velocity gradient of the microsheet might be expected to play a role in the particles size distributions as well as the microsheet thickness.

3.) Though much progress has been made in the software development for analysis of the holography data, there are still areas that have been identified that need to be improved. These improvements will provide more accurate extraction of the particles from the image data. The improved analysis will be applied to current and future image data sets.

5. CONCLUSIONS.

In this report, a high-resolution UV in-line Fraunhofer holography diagnostic has been described. Significant improvements made to the diagnostic have been discussed, including the laser system, lens system, and the analysis procedure. In addition, a HE driven shock physics platform has been designed so that many ejecta experiments can be conducted in a cost effective manner, in which the lens system survives the experiment. One to two experiments can be conducted per day with a team of five people. The final upgrades to the system were completed in fiscal year 2013 with the addition of a spatial filter to the high-powered laser. Since that time, data has been acquired investigating the details of microsheet breakup and the particle size distributions that proceed for a variety of groove geometries in a vacuum environment. Some of these data have been presented in this report for one particluar groove geometry. An outstanding question for some time has been how the ejecta particle size distribution varies as a function

of ejecta velocity. With this new experimental platform, for the first time, ejecta particle-size distributions have been obtained over the entire ejecta velocity distribution. These results have been presented for ejecta produced from a microsheet and show that for much of the velocity range, the distribution changes slowly, where the average particle size goes from approximately 3.5 μm in diameter to 4.5 μm in diameter for values of v_e/v_{fs} of 1.7 and 1.3 respectively. Below v_e/v_{fs} of 1.3 the average size changes more significantly to average diameters near 7 μm. Below v_e/v_{fs} ~ 1.1 it has been observed that the micro-sheet has not completely broken up and so in these regions, there exist both particles and tendrils. At slower velocites of v_e/v_{fs} ~ 1.05, most of the microsheet exists as web-like structures as discussed in Section 3.1.1. These data and observations will be used in testing models and corresponding physics of microsheet breakup.

It was found experimentally, that for small amount of helium gas, holograms can still be successfully produced. However, the data quality is reduced as the gas pressure increases. Reasonable holgrams were obtained up to gas pressures of 19 psia. Even with small amounts of helium gas, it was observed that the ejecta particles were breaking up, and therefore the physics of ejecta particle breakup in a gas could be studied. The first results for four different gas pressures have been presented and compared with an equivelent experiment done in a vacuum. The data show that for very small amounts of gas pressure, particle breakup is significant. The ejecta particle-size distribution obtained in a vacuum enviroment is modified by the gas interaction so that the larger part of the distribution is reduced and the smaller size part of the distribution is enhanced. This effect increases as the he gas pressure increases. Both the average particle diameter and the steepness of the distribution changes over the helium gas pressures studied in this report.

Finally, an extension of the holography diagnostic system was implemented in which a superposition of two holograms was produced on one piece of film from two laser pulses. This data allows for a direct measurement of ejecta velocity as described above. A rich set of holography data has been obtained, and the analyses are ongoing.

ACKNOWLEDGMENTS

In addition to the author list, we would like to acknowledge the support of Derek Schmidt, John Martinez, and Felix Garcia in the fabrication of the Sn samples. This work was supported by Science Campaigns 1 and 2.

REFERENCES

1. N.S.P. King et. al., 25th International Congress on High-Speed Photography and Photonics, Claude Cavailler, Graham P. Haddleton, Manfred Hugenschmidt, Editors, SPIE Vol. 4948 (2003).
2. F. Mizusako, K. Ogasawara, K. Kondo, F. Saito, H. Tamura, Rev. Sci. Instrum. **76**, 025102 (2005).
3. W. S. Vogan, W. W. Anderson, M. Grover, J. E. Hammerberg, N. S. P. King, S. K. Lamoreaux, G. Macrum, K. B. Morley, P. A. Rigg, G. D. Stevens, W. D. Turley, L. R. Veeser, and W. T. Buttler, J. Appl. Phys. **98**, 113508 (2005).
4. W. T. Buttler, R. S. Hixson, N. S. P. King, R. T. Olson, P. A. Rigg, M. B. Zellner, N. Routley, A. Rimmer, Appl. Phys. Lett. **90**, 151921 (2007).
5. C. E. Lloyd, M. W. Greenaway, and W. G. Proud, AIP Conf. Proc. 845, 1195 (2006).
6. J. R. Asay, J. Appl. Phys. **49**, 6173 (1978).
7. J. R. Asay, "Material ejection from shock-loaded free surfaces of aluminum and lead," Sandia National Laboratory Technical Report No. SAND-76-0542, 1976.
8. J. R. Asay, L. P. Mix, and F. C. Perry, Appl. Phys. Lett. **29**, 284 (1976).
9. Chandra S. Vikram, Particle Field Holography," in *Cambridge Studies In Modern Optics* (1992).
10. C. F. McMillan, R. Whipkey, " Holographic measurement of ejecta from shocked metal surfaces," SPIE 1032 High Speed Photography and Photonics 553 (1988)
11. D.S. Sorenson, R.M. Malone, B.C. Frogget. C. A. Ciarcia, T.W. Tunnell, R. L. Flurer, "Particle distribution measurements using in-line Fraunhofer holography," Proc. SPIE **2869**, 206–213 (1997).
12. D. S. Sorenson, R. W. Minich, J. L. Romero, T. W. Tunnell, and R. M. Malone, J. Appl. Phys. **92**, 5830 (2002).
13. O.T. Strand, et al., *Rev. Sci. Instrum.*, **77**, 083108 (2006)..
14. Malone, R. M., Capelle, G. A., Cox, B. C., Frogget, B. C., Grover, M., Kaufman, M. I., Pazuchanics, P., Sorenson, D. S., Stevens, G. D., Tibbitts, A., and Turley, W. D., "Design, Assembly, and Testing of a High-Resolution Relay Lens used for Holography with Operation at both Doubled and Tripled Nd:YAG laser Wavelengths," *SPIE Optics & Photonics Conference*, Proc. SPIE 7433, 7330L, (2009). DOI:10.1117/12.825812.
15. Malone, R. M., Capelle, G. A., Cox, B. C., Frogget, B. C., Grover, M., Kaufman, M. I., Pazuchanics, P., Sorenson, D. S., Stevens, G. D., Tibbitts, A., and Turley, W. D., "High-Resolution UV Relay Lens for Particle Size Distribution Measurements using Holography,"

APPENDIX 1

APPENDIX 2

Shot-3, February 11, 2014. He Gas pressure = 18.75 psia